Effects of the frequency dependence of phase response curves on network synchronization

Christian G. Fink[1], Victoria Booth[2], and Michal Zochowski[1,3]
[1]Department of Physics, [2]Departments of Mathematics and Anesthesiology, [3]Biophysics Program

University of Michigan
Ann Arbor, MI 48109

1 Abstract

Neuronal phase response curves (PRCs) generally fall into one of two classes. Type I PRCs exhibit exclusively phase advances and lead to decreased propensity for synchronization of excitatory networks, while Type II PRCs show regions of both phase delay and phase advance and better facilitate synchronization of excitatory networks. One little-investigated feature of neuronal PRCs is that they are attenuated as neuronal firing frequency increases. Interestingly, Type II PRCs often experience greater attenuation of their phase delay region compared to their phase advance region, while Type I PRCs typically show uniform attenuation of phase shifts. We simulate large-scale excitatory networks of Morris-Lecar neurons in order to investigate the effects of these phenomena upon network synchrony, and we show that they lead to Type I network synchrony *increasing* with increased frequency and Type II network synchrony *decreasing* with increased frequency.

2 Introduction

It is well known that individual neurons respond differently to external stimulation. Different response properties are primarily due to different excitation properties of the neuronal membrane, but differences in the anatomical structure of the neurites can also contribute (Schultheiss et al., 2010). Two basic measures characterizing general response properties of individual neurons are the frequency-current (f-I) curve and the phase response curve (PRC). The f-I curve measures neuronal firing frequency in response to continuous stimulation by external current. Typically, neurons can be divided into two groups based on their f-I curves, Type I and Type II (see Fig. 1(a)). The frequency of Type I neurons is strongly modulated by the magnitude of the external current and can take on very low values at firing threshold. The frequency of Type II neurons is much less responsive to changes in the current magnitude. These neurons start firing at threshold with a critical frequency and as current amplitude increases, firing frequency does not change as significantly.

The neuronal PRC is an experimentally obtainable measure characterizing the response of a periodically firing neuron to brief, weak external stimulation. The PRC is calculated as the time difference between the firing of the neuron when it is perturbed by the external pulse relative to its firing when it is unperturbed:

$$\Delta = \frac{T - T_{new}(\theta)}{T}, \tag{1}$$

where $\theta = t/T$ denotes the normalized phase of the neuron when the external pulse is applied (with $\theta \equiv 0$ at a voltage peak), t is the time of pulse application, T is the firing period of the unperturbed

neuron and T_{new} is the period of a perturbed cycle. Thus, the value of Δ is negative if the perturbed period is longer than the unperturbed one (constituting a phase delay) and, conversely, it is positive if the perturbed period is shorter than the unperturbed one (constituting a phase advance). Neuronal PRCs have also been divided into two groups. Type I PRCs show phase advances for almost all stimulus phases, while Type II PRCs show a region of phase delay for early stimulus phases and a region of phase advance for late stimulus phases. Conveniently, neurons with Type I f-I curves typically have Type I PRCs and neurons with Type II f-I curves typically have Type II PRCs (Ermentrout, 1996).

Properties of PRCs and their implications for neuronal responses have been studied extensively for single neurons as well as for small networks composed of a few cells (Hansel et al., 1995; Ermentrout, 1996; Canavier et al., 1997; Dror et al., 1999; Maran and Canavier, 2008; Luo et al., 2004). Theoretical results have shown that neurons with Type II PRCs tend to synchronize more readily when synaptically coupled compared to neurons with Type I PRCs (Hansel et al., 1995; Ermentrout, 1996). This may generally be attributed to the absence of a phase delay region in the Type I PRC, which leaves Type I neurons with only one method of adapting to the signal of a coupled neuron. For a heuristic explanation of this phenomenon, see Fig. 2. Despite the progress that has been made in understanding the effects of PRCs upon network synchronization, it remains unclear how the shape of the PRC influences spatio-temporal activity in larger networks. Recently, we have shown using numerical simulations that the PRC of individual neurons is indeed a good predictor of synchronization in large networks (Bogaard et al., 2009). Specifically, we studied spatio-temporal activity patterns in large-scale excitatory networks composed of biophysically accurate model neurons exhibiting both types of f-I curves and PRCs. We showed that networks consisting of neurons with Type II PRCs synchronize more easily for different network topologies and connectivity parameters. Furthermore, these neurons can drive synchronization in heterogenous networks composed primarily of neurons exhibiting Type I PRCs. While these results support the idea that the neuronal PRC can be a good predictor of synchrony in a large network, they only provide preliminary data indicating the relevance of the PRC to spatio-temporal patterning of neural activity in complex networks.

In this chapter, we first investigate links between the two measures which characterize neural response to external stimuli, then investigate their influence on network spatio-temporal activity patterns. Specifically, we measure changes in the PRC as a function of firing frequency of the neuron. We find that while the PRC of a given neuron depends on a number of factors, including the amplitude of the stimulating pulse and the firing frequency of the neuron at which the PRC is measured, for neurons with Type I PRCs these factors mainly influence the amplitude of the induced phase shifts but do not qualitatively change the profile of the PRC. However, for neurons with Type II PRCs, the amplitude of the phase delays evoked at early phases can decrease significantly as the intrinsic firing frequency increases, leading to a more Type I-like response. Thus, by modulating firing frequency, we can continuously monitor the transition from Type II to Type I-like PRCs and

observe the effect of this transition upon spatio-temporal patterning in a large network. Specifically, we consider the propensity for synchronization as a function of network firing frequency in large-scale excitatory networks composed of either Type I or Type II Morris-Lecar model neurons.

3 Type I and Type II dynamics of Morris-Lecar model neurons

In our model networks, individual neurons are modeled by the Morris-Lecar equations (Morris and Lecar, 1981),

$$C\frac{dV}{dt} = -\overline{g}_{Ca}m_\infty(V)(V-V_{Ca}) - \overline{g}_K w(V-V_K) - \overline{g}_L(V-V_L) + I_{\text{app}} \quad (2)$$

$$\frac{dw}{dt} = \phi\frac{w_\infty(V)-w}{\tau_w(V)} \quad (3)$$

$$m_\infty(V) = \frac{1}{2}\left[1+\tanh\left(\frac{\mathrm{V}-\overline{\mathrm{V}}_1}{\overline{\mathrm{V}}_2}\right)\right] \quad (4)$$

$$w_\infty(V) = \frac{1}{2}\left[1+\tanh\left(\frac{\mathrm{V}-\overline{\mathrm{V}}_3}{\overline{\mathrm{V}}_4}\right)\right] \quad (5)$$

$$\tau_w(V) = \frac{1}{\cosh\left(\frac{\mathrm{V}-\overline{\mathrm{V}}_3}{2\overline{\mathrm{V}}_4}\right)}, \quad (6)$$

where V represents membrane voltage (in mV) and time is measured in msec. Action potentials are generated by an inward Ca^{2+}-mediated current and an outward K^+-mediated current whose dynamics are governed by the gating variable w. The functions $m_\infty(V)$ and $w_\infty(V)$ are the steady state activation functions of the Ca^{2+} and K^+ currents, and $\tau_w(V)$ is the time constant governing dynamics of the gating variable w. The term I_{app} represents an externally applied stimulus to the neuron.

Following Rinzel and Ermentrout (1998), we use the parameters listed in Table 1 to simulate Type I and Type II Morris-Lecar model neurons. Fig. 1(a) depicts the f-I curves of both neuron types. Note that the frequency of the Type I neuron is capable of assuming arbitrarily low values at firing threshold, while the Type II neuron exhibits a critical frequency at threshold of about 8 Hz.

Parameter	Type I	Type II
C	20 μF/cm^2	20 μF/cm^2
g_{Ca}	4.0 mS/cm^2	4.4 mS/cm^2
g_K	8.0 mS/cm^2	8.0 mS/cm^2
g_L	2.0 mS/cm^2	2.0 mS/cm^2
V_{Ca}	120.0 mV	120.0 mV
V_K	-84.0 mV	-84.0 mV
V_L	-60.0 mV	-60.0 mV
$\overline{V}_1$	-1.2 mV	-1.2 mV
$\overline{V}_2$	18.0 mV	18.0 mV
$\overline{V}_3$	12.0 mV	2.0 mV
$\overline{V}_4$	17.4 mV	30.0 mV
ϕ	1/15	0.04
I_{app}	35.0 μA/cm^2	80.0 μA/cm^2

Table 1: Parameters for the Morris-Lecar Type I and Type II model neurons used in our simulations, taken from Rinzel and Ermentrout (1998).

Figs. 1(b,c) depict the PRCs of Type I and Type II Morris-Lecar neurons in response to excitatory stimulation. Note that at low frequency, both types exhibit a phase delay when a current pulse is applied at values of θ slightly greater than 0. This is due to the fact that $\theta = 0$ is defined to occur at maximum membrane voltage, so that the voltage naturally decreases at the beginning of the cycle, when the neuron is repolarizing after an action potential. The excitatory applied current pulse therefore opposes this process and delays the natural oscillatory behavior. In the Type I neuron, this initial phase delay gives way to phase advance for stimulation at later phases in the firing cycle. The Type II neuron exhibits qualitatively different behavior. The initial phase delay region is followed by a further delay region, forming a second, larger "trough" before finally giving way to a phase advance region at late phases of stimulation.

3.1 Frequency Dependence of PRCs

In the Morris-Lecar model, PRC properties are strongly affected not only by the properties of membrane excitability but also by the induced firing frequency of the unperturbed neuron. Figs. 1(b,c) depict changes in the phase shifts for both types of neurons as the firing frequency of the neuron is increased by increasing the external current I_{app}. In both cases, there is an overall attenuation of the PRC as frequency increases. Additionally, the Type II PRC exhibits an extreme attenuation of the phase delay region relative to the phase advance region with increased frequency, rendering the neuron more Type I-like. This phenomenon is quantified in Fig. 3.

4 Network Model

To better understand the effects on network dynamics of frequency-dependent changes in the characteristics of the PRC, we simulated large-scale excitatory networks consisting of either Type I or Type II Morris-Lecar neurons for different average network firing frequencies. We varied synaptic weight and network connectivity and then quantified synchronization of the network spatio-temporal activity patterns.

4.1 Network structure

In our networks of Morris-Lecar neurons, individual neurons are in an excitable state (I_{app} levels are set below firing threshold) and underlying network activity is driven by random, excitatory noise to each neuron. Thus, we modify equation (2) for the membrane voltage of the $\imath$th neuron $V_\imath$ as follows:

$$C\frac{dV_\imath}{dt} = -\overline{g}_{Ca}m_\infty(V_\imath)(V_\imath - V_{Ca}) - \overline{g}_K w_\imath(V_\imath - V_K) - \overline{g}_L(V_\imath - V_L) + I_{\text{app}} + \sum_{\jmath\in\Gamma_\imath} I_{\imath\jmath}^{\text{syn}} + I_\imath^{\text{noise}}. \quad (7)$$

Here we have added two terms, one for the synaptic current exchanged between neurons, $\sum_{\jmath\in\Gamma_\imath} I_{\imath\jmath}^{\text{syn}}$, and another for random, excitatory inputs used to modulate average network firing frequency, $I_\imath^{\text{noise}}$. The synaptic current flowing from neuron $\jmath$ to $\imath$ is defined to be non-zero if neuron $\jmath$ is directionally coupled to neuron $\imath$ (i.e., $\jmath \in \Gamma_\imath$) and the voltage of neuron $\jmath$ is greater than 0 mV. The magnitude of the synaptic current is given by

$$I_{\imath\jmath}^{\text{syn}} = s\,\max(0, \mathrm{V}_\jmath). \quad (8)$$

The synaptic weight s is the same for all synapses, and its specific value is one of the parameters varied from simulation to simulation.

The term I^{noise} is used to control the average firing frequency of the network. Each neuron randomly receives square current pulses of amplitude 300 μA/cm^2 and duration 0.5 msec at a specified frequency. The noise frequency determines the average firing frequency of the network. Additionally,

Type I and Type II neurons are both given sub-threshold baseline currents, with $I_{\text{app}} = 35\,\mu\text{A/cm}^2$ for Type I and $I_{\text{app}} = 80\,\mu\text{A/cm}^2$ for Type II, to compensate for their differences in threshold current.

The neurons are connected in a one-dimensional network with periodic boundary conditions. The connectivity pattern is constructed using the Watts-Strogatz architecture for Small World Networks (Watts and Strogatz, 1998) . A radius of connectivity r is specified, and each neuron is directionally coupled to its $2r$ nearest neighbors. Then, every connection in the network is rewired with probability p to another neuron chosen at random. In this way, $p = 0$ results in a locally-connected network and $p = 1$ in a randomly connected network. The radius of connectivity r therefore determines the density of connections in the network, while the re-wiring probability p determines the network connectivity structure. r is set to 5 for all simulations except those used to generate Fig. 6. All simulated networks have 250 neurons.

4.2 Measuring network synchronization

We monitor phase-synchronization of firing in the network using the mean phase coherence, σ (Mormann et al., 2000). The mean phase coherence between a pair of neurons, $\sigma_{1,2}$, is defined by:

$$\sigma_{1,2} = \left| \frac{1}{N} \sum_{k=1}^{N} e^{i\phi_k} \right| \tag{9}$$

$$\phi_k = 2\pi \left(\frac{t_{2,k} - t_{1,k}}{t_{1,k+1} - t_{1,k}} \right), \tag{10}$$

where $t_{2,k}$ is the time of the k^{th} spike of neuron 2, $t_{1,k}$ is the time of the spike of neuron 1 that is largest while being less than $t_{2,k}$, $t_{1,k+1}$ is the time of the spike of neuron 1 that is smallest while being greater than or equal to $t_{2,k}$, N is the number of spikes of neuron 2, and $e^{i\phi_k} = \cos(\phi_\text{k}) + i\sin(\phi_\text{k})$. The mean phase coherence of the entire network, σ, is calculated by averaging $\sigma_{i,j}$ over all pairs of neurons, excluding $\imath = \jmath$.

5 Effects of the PRC Frequency Dependence on Network Synchronization

We investigated the changes in network mean phase coherence as a function of network structure for different values of average frequency of network activity. Figs. 4(a-c) summarize the dual effects of synaptic coupling and architecture on synchronization of Type I networks. For low coupling strengths s (vertical axis), the networks essentially fail to synchronize regardless of the value of the rewiring probability p (horizontal axis), indicated by the low values of mean phase coherence. Above $s \approx 0.3$ mS/cm^2, however, the networks synchronize for network architectures with a large fraction of random connectivity. Fig. 4(c) shows that the differences in mean phase coherence between networks driven at high frequencies and low frequencies, $\sigma_{\text{high}} - \sigma_{\text{low}}$, are positive, revealing that Type I networks synchronize better at higher frequency. This is hardly a surprising result, because higher network frequency implies more exchange of synaptic current, which leads to greater effective coupling among neurons. For $s \gtrsim 0.45$mS/cm^2, the differences in mean phase coherence, $\sigma_{\text{high}} - \sigma_{\text{low}}$, return to approximately 0, since σ saturates for both the high- and low-frequency networks at such high coupling.

Type II networks, on the other hand, exhibit quite different behavior. Results depicted in Figs. 4(d-f) demonstrate that appreciable network synchronization occurs at coupling strengths of $s \approx 0.2$mS/cm^2 and greater. At the same time, the differences in mean phase coherence between networks driven at high frequency and at low frequency, $\sigma_{\text{high}} - \sigma_{\text{low}}$, remain negative, implying that Type II networks synchronize better at *lower frequency* (see Fig. 4(f), and note the difference in scale from Fig. 4(c)). These results differ from those obtained for Type I networks, in which synchrony increases with increasing mean network firing frequency. This contrast in synchronization behavior is even more clearly illustrated in Fig. 5, where the differences in mean phase coherence between high- and low-frequency networks are plotted as a function of synaptic weight for a number of different pairings of noise frequency. In all cases, the difference in synchronization between high- and low-frequency Type I networks starts at essentially zero, steeply rises to a large peak as synaptic weight increases, then returns to zero as both networks saturate. The presence of this pronounced region of positively-valued $\sigma_{\text{high}} - \sigma_{\text{low}}$ for all frequency pairings demonstrates the tendency of Type I networks to synchronize better at higher frequency. Type II networks, on the other hand, exhibit large regions of negative $\sigma_{\text{high}} - \sigma_{\text{low}}$ for all frequency pairings, indicating that Type II networks tend to synchronize better at lower frequency. Interestingly, Figs. 5(c,d) show a small region where $\sigma_{\text{high}} - \sigma_{\text{low}}$ is significantly positive for Type II networks. This feature is lacking in Figs. 5(a,b). These contrasting results may be a result of the competing influences of effective coupling and PRC phase delay. As frequency increases, more current is exchanged between neurons, leading to higher effective coupling and increased synchronization. At the same time, increasing frequency also leads to a diminishing phase delay region in the neuronal PRCs, which depresses synchronization. The interplay between these two influences is nontrivial, and we see that in Figs. 5(a,b) the depressive

pressure of the neuronal PRC dominates for virtually all values of s, while in Figs. 5(c,d) the positive pressure of effective coupling dominates for small synaptic weight values, before giving way to the effects of the neuronal PRC at greater values of s.

We obtain similar results when considering cross sections of the color plots from Figs. 4(a-f). In Figs. 4(g,h) the synaptic coupling is fixed and the mean phase coherence is plotted as a function of re-wiring probability p for four different noise frequencies. The strength of synaptic coupling was chosen to lie in a transitional region, where Type I network synchrony takes on an intermediate value ($s = 0.36$ mS/cm^2). In both Type I and Type II networks, mean phase coherence increases with increasing re-wiring probability, but increasing frequency affects the two types of networks in different ways. In the Type I network (Fig. 4(g)), higher frequency implies greater σ values for all values of p, while in the Type II network (Fig. 4(h)) higher frequency yields slightly smaller σ values for virtually all values of p. This effect in the Type II network is not due to changes in network firing frequency with changes in p, since average network firing frequency remains virtually constant for all values of p (Fig. 4(i)). These results further indicate that for networks of Type II neurons, the increase in network propensity for synchronization due to higher mean firing frequency, and thus higher effective coupling, is offset by reduced cellular propensity for synchronization.

We also investigated how network connection density affects the emergence of network synchrony for the two network types. Figs. 6(a) and 6(b) depict the differences in mean phase coherence for high- and low-frequency network firing, $\sigma_{\text{high}} - \sigma_{\text{low}}$, as a function of p and the radius of connectivity r, for Type I and Type II networks, respectively. Similar to our previous results in which Type I networks exhibited positive values of $\sigma_{\text{high}} - \sigma_{\text{low}}$ for a bounded range of coupling strength values (Fig. 4(c)), Type I networks also show greater synchrony at high frequency than at low frequency between $r \approx 5$ and $r \approx 7$. Type II networks synchronize slightly better at low frequency than at high frequency for $r \gtrsim 2$, which is analogous to the transition that occurs at $s \approx 0.2$ mS/cm^2 in Fig. 4(f). These results show that the networks behave in qualitatively the same manner for both increasing r and increasing s, which is not surprising, since the effect of both is a greater exchange of synaptic current within the network.

6 Conclusion

The aim of this chapter has been to show the link between frequency modulation of the neuronal PRC and propensity for network synchronization. We investigated these links in the Morris-Lecar neuronal model under two standard excitability regimes, Type I and Type II excitability. For each cell type, as the intrinsic firing frequency of our model neurons increases, phase shifts in spike timing (as measured by the PRC) decrease. This attenuation is uniform across all phases for the Type I

cell but not for the Type II cell, which exhibits a greater attenuation of the phase delay region than of the phase advance region. We have investigated the effect of this frequency-dependent, gradual abolition of the phase delay region of Type II PRCs upon network synchronization. In large, noisy, excitatory networks, we have varied synaptic weight and connectivity architecture across parameter regimes that both prevent and promote network synchronization. As average network firing frequency is increased by changing the frequency of random excitatory inputs, we observe diminished synchronization (as measured by mean phase coherence) in networks composed of Type II neurons. This phenomenon is robust and can be attributed to the non-uniform, pronounced attenuation of phase delays in Type II neurons as frequency increases. In contrast, networks composed of Type I neurons, whose PRCs have no delay region and are uniformly attenuated as frequency increases, show an increase in propensity for synchronization as frequency increases.

These results paint a complex picture of interactions between network and cellular properties that may lead to nontrivial effects in terms of network dynamical patterns. For example, neurons having various intrinsic cellular properties may be differentially mixed to form networks having different capacities in terms of their pattern formation. As we have shown, Type I networks have a stronger propensity to synchronize at high compared to low frequencies, whereas Type II networks show the opposite tendency. It is therefore possible that Type I networks function as integrators, while Type II networks may act as low-pass filters in the temporal coding regime.

References

Bogaard, A., Parent, J., Zochowski, M., and Booth, V. (2009). Interaction of cellular and network mechanisms in spatiotemporal pattern formation in neuronal networks. *The Journal of Neuroscience*, 29:1677–1687.

Canavier, C., Butera, R., Dror, R., Baxter, D., Clark, J., and Byrne, J. (1997). Phase response characteristics of model neurons determine which patterns are expressed in a ring circuit model of gait generation. *Biological Cybernetics*, 77:367–380.

Dror, R., Canavier, C., Butera, R., Clark, J., and Byrne, J. (1999). A mathematical criterion based on phase response curves for stability in a ring of coupled oscillators. *Biological Cybernetics*, 80:11–23.

Ermentrout, B. (1996). Type i membranes, phase resetting curves, and synchrony. *Neural Computation*, 8:979–1001.

Hansel, D., Mato, G., and Meunier, C. (1995). Synchrony in excitatory neural networks. *Neural Computation*, 7:307–337.

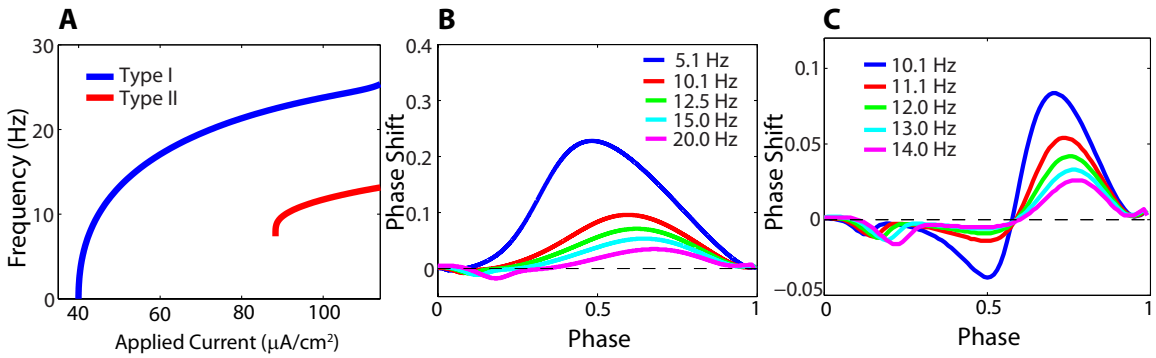

Figure 1: (a) Frequency-current (f-I) curves for Type I and Type II Morris-Lecar neurons. The firing frequency of the Type I neuron goes to zero at firing threshold, while the Type II neuron exhibits a threshold frequency of about 8 Hz. (b) PRCs for various firing frequencies of the Type I Morris-Lecar neuron. PRCs were calculated using 0.5 msec excitatory current pulses of amplitude 200 μA/cm^2. (c) PRCs for various firing frequencies of the Type II Morris-Lecar neuron. PRCs were calculated using 0.5 msec excitatory current pulses of amplitude 200 μA/cm^2.

Luo, C., Clark, J., Canavier, C., Baxter, D., and Byrne, J. (2004). Multimodal behavior in a four neuron ring circuit: Mode switching. *IEEE Transactions on Biomedical Engineering*, 51:205–218.

Maran, S. and Canavier, C. (2008). Using phase resetting to predict 1:1 and 2:2 locking in two neuron networks in which firing order is not always preserved. *Journal of Computational Neuroscience*, 24:37–55.

Mormann, F., Lehnertz, K., David, P., and Elger, C. (2000). Mean phase coherence as a measure for phase synchronization and its application to the eeg of epilepsy patients. *Physica D-Nonlinear Phenomena*, 144:358–369.

Morris, C. and Lecar, H. (1981). Voltage oscillations in the barnacle giant muscle fiber. *Biophysical Journal*, 35:193–213.

Rinzel, J. and Ermentrout, B. (1998). Analysis of neural excitability and oscillations. In Koch, C. and Segev, I., editors, *Methods in Neuronal Modeling*. MIT Press.

Schultheiss, N., Edgerton, J., and Jaeger, D. (2010). Phase response curve analysis of a full morphological globus pallidus neuron model reveals distinct perisomatic and dendritic modes of synaptic integration. *The Journal of Neuroscience*, 7:2767–2782.

Watts, D. and Strogatz, D. (1998). Collective dynamics of "small-world" networks. *Nature*, 393:440–442.

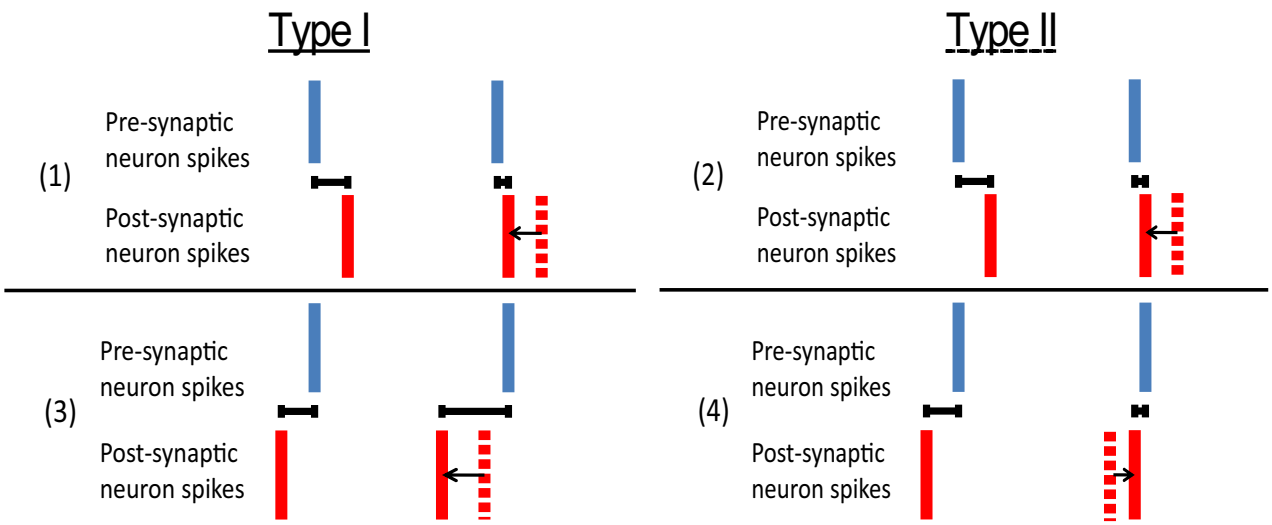

Figure 2: Heuristic explanation of why excitatory neurons with Type II PRCs have a greater propensity for synchronization than excitatory neurons with Type I PRCs. Consider two neurons coupled with a unidirectional excitatory synapse and being driven to fire periodically at similar frequencies. For cases (1)-(4), vertical ticks represent spike times of the pre-synaptic (blue) and the post-synaptic (red) neuron during an unperturbed cycle (dashed tick) and a perturbed cycle (solid tick, with black arrows indicating the change in spike time). In cases (1) and (2), the pre-synaptic neuron fires near the end of the post-synaptic neuron's oscillatory cycle, which induces a phase advance in both Type I and Type II neurons. The phase advance results in the post-synaptic spike occurring closer in time to the next pre-synaptic spike, thereby enhancing synchrony. In cases (3) and (4), the pre-synaptic neuron fires near the beginning of the post-synaptic neuron's oscillatory cycle. This induces a phase advance in the Type I post-synaptic neuron but a *phase delay* in the Type II post-synaptic neuron. The phase advance of the Type I neuron increases the separation in time between spikes of the pre- and post-synaptic neurons, resulting in diminished synchrony. In contrast, the phase delay of the Type II neuron decreases the separation in time between spikes of the pre- and post-synaptic neurons, resulting in enhanced synchrony. Thus, input to Type II neurons at both early and late phases promotes synchrony, while input to Type I neurons only promotes synchrony when received at late phases.

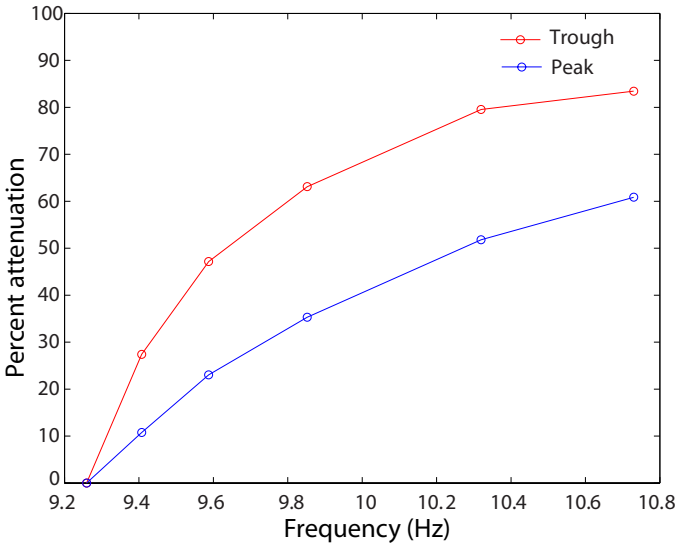

Figure 3: Attenuation of both the peak and trough of the Type II PRC as a function of frequency, relative to the amplitudes of the peak and trough when the neuron is firing at approximately 9.3 Hz. PRCs were computed using 0.5 msec current pulses of amplitude 40 μA/cm^2.

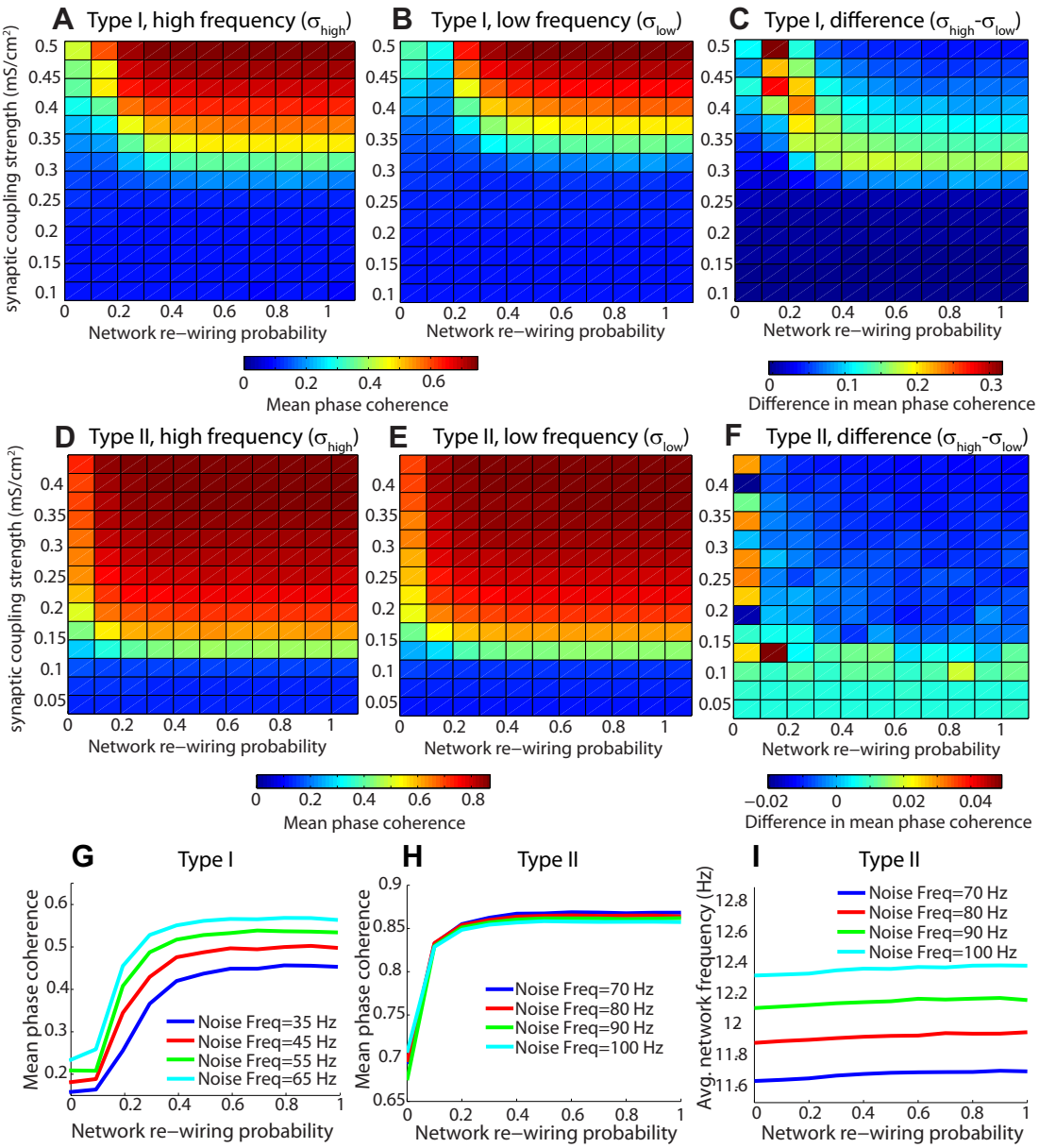

Figure 4: (a,b) Mean phase coherence σ as a function of synaptic coupling strength s and re-wiring probability p for networks of Type I neurons driven with a noise frequency of 65 Hz (σ_{high}, a) and of 35 Hz (σ_{low}, b). (c) Difference between the σ values for the high-frequency and low-frequency Type I networks, $\sigma_{\text{high}} - \sigma_{\text{low}}$, as a function of synaptic coupling strength s and re-wiring probability p. (d,e) Mean phase coherence σ as a function of synaptic coupling s and re-wiring probability p for networks of Type II neurons driven with a noise frequency of 100 Hz (σ_{high}, d) and of 70 Hz (σ_{low}, e). (f) Difference between the σ values for the high-frequency and low-frequency Type II networks, $\sigma_{\text{high}} - \sigma_{\text{low}}$, as a function of synaptic coupling strength s and re-wiring probability p. Note the difference in scale between (c) and (f). (g) Cross sections of (a) and (b) with additional, intermediate frequency stimulation values and s fixed at 0.36mS/cm^2. (h) Cross sections of (d) and (e) with additional, intermediate frequency stimulation values and s fixed at 0.36mS/cm^2. (i) Average network firing frequency as a function of p for various values of the noise frequency in a Type II network, with $s = 0.36$mS/cm^2.

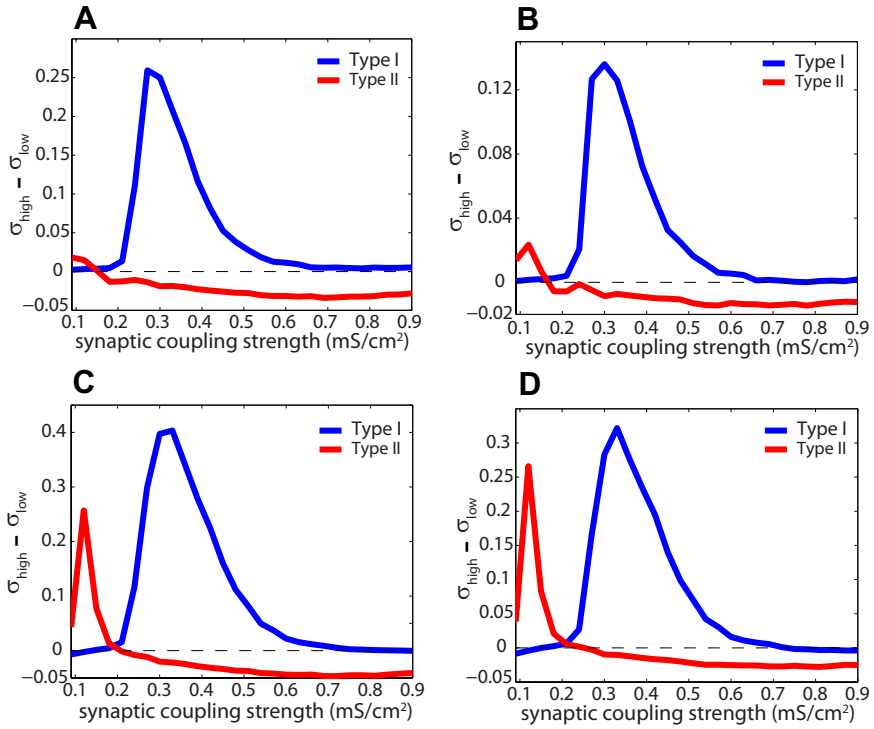

Figure 5: Difference in mean phase coherence, $\sigma_{\text{high}} - \sigma_{\text{low}}$, as a function of synaptic coupling s for Type I (blue) and Type II (red) networks driven at high and low noise frequencies of (a) 130 Hz and 60 Hz, (b) 90 Hz and 60 Hz, (c) 130 Hz and 30 Hz, and (d) 90 Hz and 30 Hz, respectively. The network re-wiring probability p is fixed at 0.3.

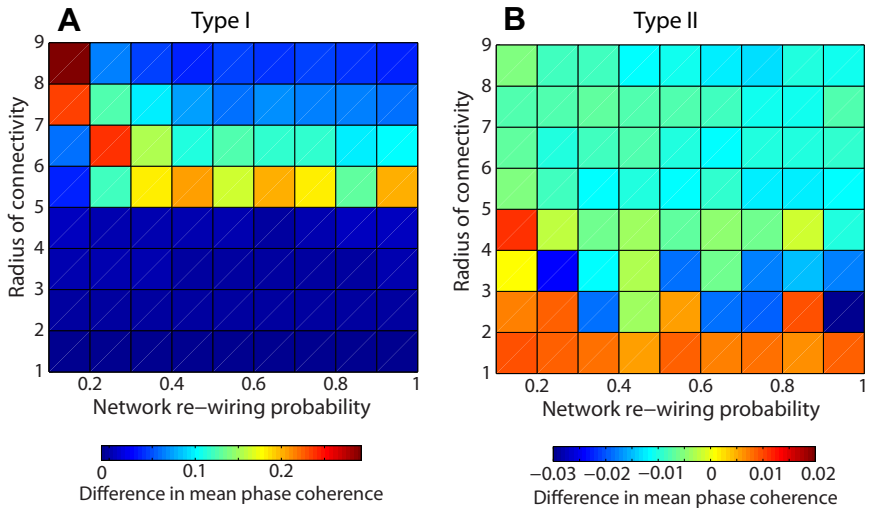

Figure 6: (a) Difference in mean phase coherences, $\sigma_{\text{high}} - \sigma_{\text{low}}$, as a function of the radius of connectivity r and the re-wiring probability p in a Type I network. s is fixed at 0.30 mS/cm^2, and the noise frequency is 65 Hz in the high frequency network and 35 Hz in the low frequency network. (b) $\sigma_{\text{high}} - \sigma_{\text{low}}$ as a function of r and p in a Type II network. s is fixed at 0.30 mS/cm^2, and the noise frequency is 100 Hz in the high frequency network and 70 Hz in the low frequency network.